Determining satellite rotation rates for unresolved targets using temporal variations in spectral signatures

Joseph Coughlin
Stinger Ghaffarian Technologies
Colorado Springs, CO
joe.coughlin@sgt-inc.com

ABSTRACT

Analyzing temporal variations in spectral signatures is a potential tool to determine the rotation rates, spin axes, and attitude of satellites from unresolved spectral images. By calculating rotational information, analysts can define the satellite in terms of its space object taxonomy [1]. This research presents an evaluation of whether temporal pattern matching techniques can be used to determine the rotation rates of satellites. This investigation uses detailed models to simulate satellite signatures in the visible and near infrared as seen by a hypothetical ground sensor. At each time step, spectral and photometric images are averaged to yield unresolved images as the satellite is propagated through the field-of-view. For each image, a material pattern map is generated based on either material identification or spectral similarity. Using techniques similar to those used to determine the rotations of asteroids from fragmented light curves, we determine satellite rotation rate and spin axes. For unresolved targets, this approach uses the periodic changes in the irradiance but evaluates the additional information available from the spectra. Previous work [2] has shown the utility of spectral material mapping for satellite anomaly detection. This research continues that effort by investigating satellite rotation and attitude information.

1. APPROACH

This study is an attempt to determine how spectral signature analyses can help characterize satellite status, primarily satellite attitude and rotation rates. Unlike previous efforts which have concentrated on specific spectral bands or total radiance, this study utilizes the entire spectral content.

For this study, we simulate the spectral signatures from different rotating targets and:
1) Evaluate the radiance as a function of time
2) Determine probable rotation rates
3) Examine the spectral signature maps derived from spectral similarity algorithms as they change over time and determine if it provides clarity in the satellite categorization

The simulation of the satellite spectral signatures is performed using SGT's Spectral Data Exploitation Workbench (SDEW), [3,4] which consists of four main components: the Emission Spectra (ES) tool which performs atmospheric radiative transfer, a three-dimensional Scenario Generation tool, an Image Processing tool for spectral image processing, and RETRV for atmospheric retrievals, as shown in Fig. 1. The SDEW software suite is tailored for the simulation, analysis, and exploitation of hyperspectral and ultraspectral data.
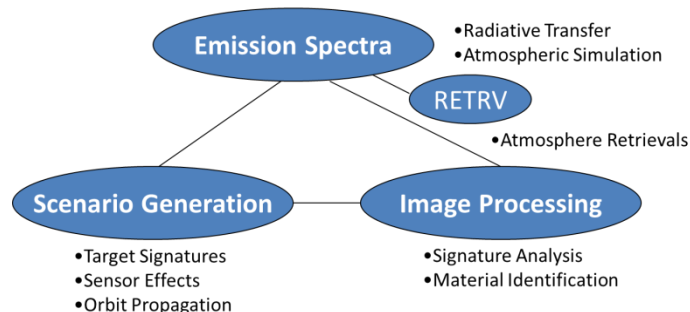
Simulation and Analysis Environment

Fig. 1. Spectral Data Exploitation Workbench Simulation Environment

The ES [5] software component is used for the computation of atmospheric transmission and thermal emission. For our analysis, it is used to compute solar reflection and thermal emission from realistic materials as well as the atmospheric radiance and transmission. The reflective and emissive spectral material properties are from an Air Force database. ES covers the spectral regions from the ultraviolet (UV) to the long wave infrared (LWIR). It utilizes the High Resolution Transmission (HITRAN) molecular database of spectroscopic line absorption parameters to calculate the line-by-line atmospheric radiative transfer. Computations at line-by-line spectral resolution ensures that the radiance and transmission calculations are the most accurate possible.

The Scenario Generation component within the SDEW computes the spectral signatures for faceted models. Coupled with the ES atmospheric radiative transfer algorithm, it computes highly accurate simulations of solar reflectance and material thermal emittance, depending on the spectral region. When computing spectral signatures from satellites, the Scenario Generator computes the position for the satellite with respect to a ground sensor and the sun using standard orbital propagators. The facet angle relative to the sun and ground is used in the computation of both the solar reflection as well as the thermal signature. The material properties, such as reflectance, emissivity, and bi-directional reflection, of the individual facets used a standard material database. The results from the Scenario Generator are convolved with sensor properties, such as pixel size, to simulate the spectral signatures observed by a sensor.

The Image Processing component within the SDEW is used to perform spectral similarity calculations. It uses some common algorithms, such as a Spectral Angle Mapper (SAM) [6] and a binary comparator, to determine how close one spectrum comes to another. This allows us to determine similar materials within the spectral image and compare them across time to calculate the rate of rotation of satellites. The knowledge of what similar materials are visible over time can help determine likely structure in unresolved images.

2. RESULTS

To verify the spectral simulation and rotation algorithms work, we started with a simple 1m^2 flat plate composed of two different materials, Kapton and cloth blanket material. For simplicity, the flat plate satellite is placed in a stationary position 1000 km above the site, which is located at 0 degrees longitude and 0 degrees latitude, as shown in Fig. 2. Fig. 2 also shows a result of the spectral radiance calculation from the flat plate. The image shows the flat plate as viewed from the site. Below the image is the spectrum of the flat plate. For more complicated shapes, this shows the spectrum from a selected facet.
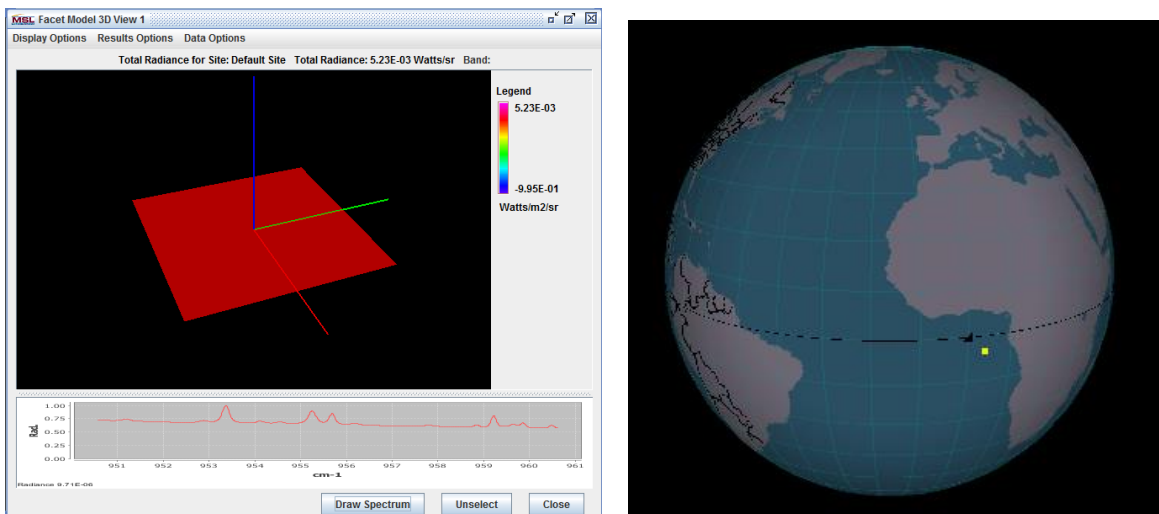

Fig. 2. Spectral radiance for a flat plate and viewing geometry

The spectral image is pixilated to represent what could be seen by a theoretical sensor, as shown in Fig. 3. Pixels are blended from the original image to yield a composite spectrum of the different materials. A background radiance spectrum is computed using only the atmosphere. This simulates the radiance in the image denoted by the black color and is used in the pixel blending. As will be seen, this background radiance can be a significant contribution to the radiance seen by the sensor in the thermal infrared.

Pixelization of the spectral image yields an unresolved image that will be used in subsequent analysis and pattern matching.

Fig. 3. Pixilated image of flat plate

The simulation can be set to rotate about any arbitrary axis. For the purpose of this test, the satellite is set to rotate about the x-axis, shown in red in Fig. 2. Spectra are computed at 10 second increments for a duration of 30 minutes and the total radiance as a function of time is shown in Fig. 4. The spectral radiances are computed at 10.5-10.6 microns at 0.1 cm^{-1} spectral resolution. In this spectral region the variations in the spectral signatures of the materials is not very large, so this analysis is likely to be a stressing case of using spectral similarity to differentiate signatures. Also it is sufficient to evaluate algorithms to determine the rotation.
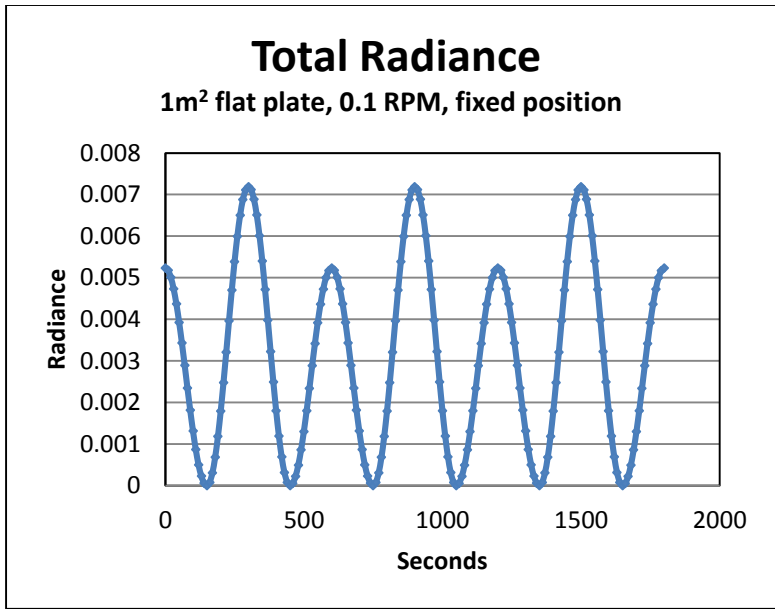
Fig. 4. Radiance as a function of time for the rotating satellite

The flat plate has different materials on either side so the resultant radiance varies by the reflectivity/emissivity. With a simulated rotation rate of 0.1 RPM, the derived 600 second periodicity validates the approach.

The satellite is next placed in a more realistic rotating configuration about the x-axis (red in Fig. 2) with the x-axis pointed toward the direction of motion along the orbit. For the modeling effort, a notional sensor is positioned at 0 degrees latitude and 0 degrees longitude. A circular orbit with a mean motion of 10 is chosen which passes within view of the site, while not going directly overhead, as shown in Fig. 5. The orbit has a 45 degree inclination and the simulation goes from horizon to horizon.
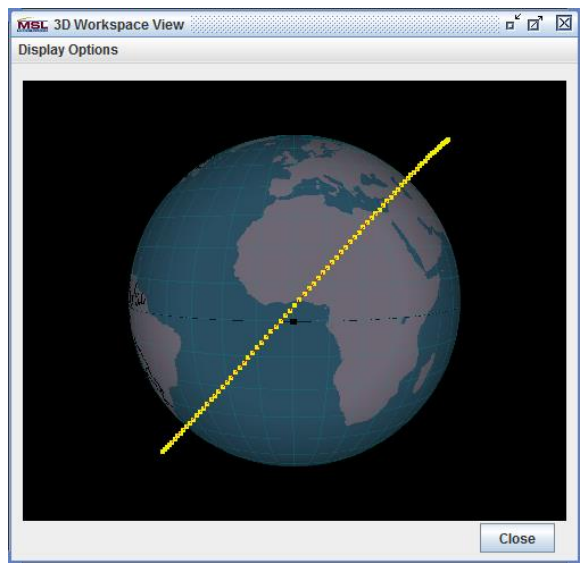

Fig. 5. Viewing geometry

The atmospheric radiance and transmission are calculated at each point along the orbit for the exact geometry of the sensor and satellite. The radiance is calculated every 60 seconds while the satellite is visible from the sensor. The total radiance is shown in Fig. 6.
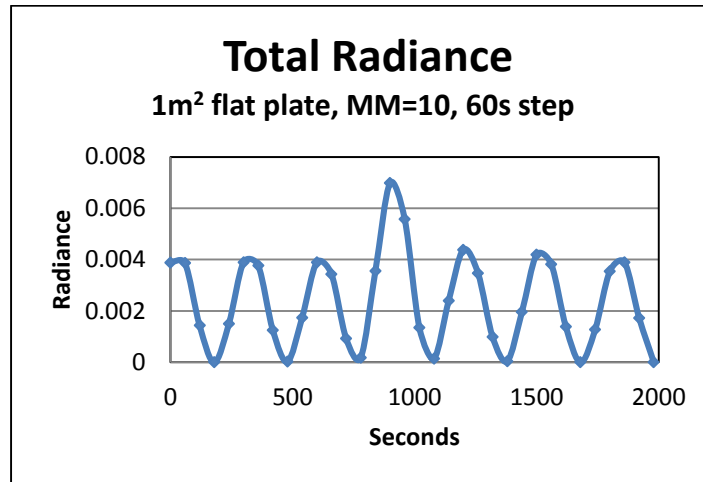
Fig. 6. Total radiance as a function of time for satellite

With a simulated rotation rate of 0.1 RPM, the derived 600 second periodicity further validates this simplistic approach to deriving rotation rates. The peak in the center corresponds to the time of closest approach to the site. We have noted that in different runs, the radiance curves can vary significantly depending on the rotation of the flat plate and its position along the orbit relative to the sensor.

However, setting the rotation rate to 0.01 RPM and propagating the plate over the site, as shown in Fig. 7, does not yield conclusive results due to the shortness of the pass. The secondary peak is where the slowly rotating satellite shows the other side before going out of coverage. Also, depending on other conditions, these radiance curves can vary considerably. Other information will be necessary to derive correct satellite attitude and rotation.
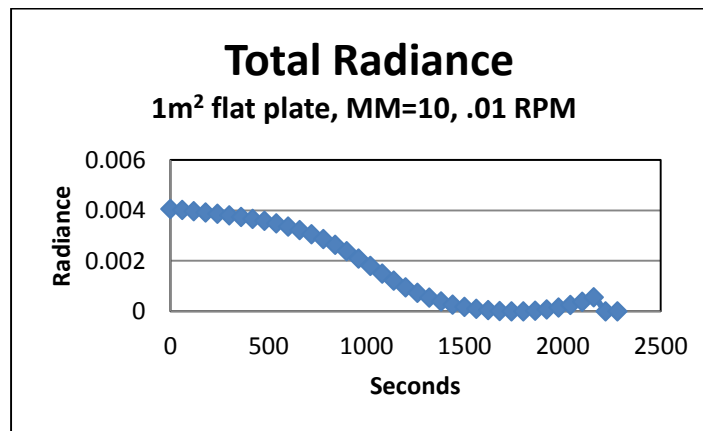

Fig. 7. Flat plate at 0.01 RPM

Performing the analysis with more complicated shapes such as a tetrahedron of different materials shows more interesting behavior. The initial radiance for the tetrahedron as visible from site is shown in Fig. 8.
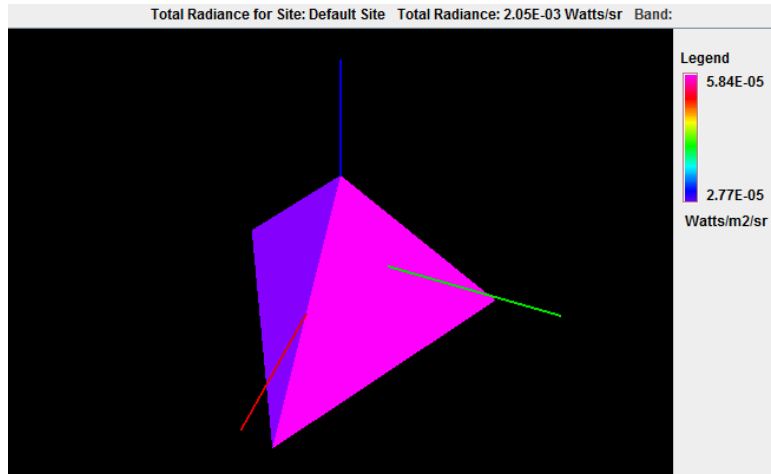
Fig. 8. Tetrahedron initial radiance

Fig. 9 shows the pixilated radiance image for the tetrahedron which is used in the analysis.
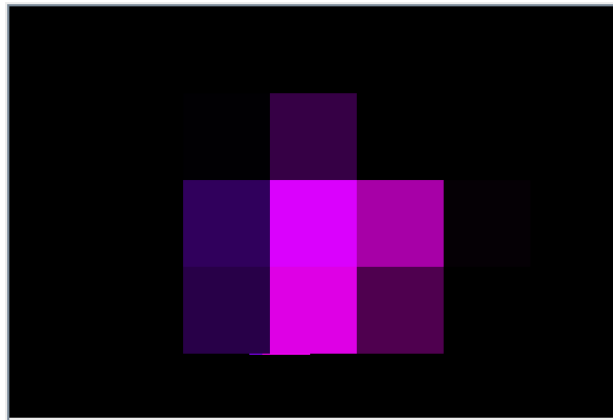

Fig. 9. Pixilated radiance image for tetrahedron satellite

Computing the radiance as a function of time as in the previous case gives the radiance curve shown in Fig. 10. As in the previous simulation, the satellite has an orbit with a mean motion of 10 but is now rotating about the z-axis, the blue line in Fig. 8, at 0.1 RPM. With the z-axis pointed toward nadir, the tetrahedron is effectively rotating with the "point" downward.
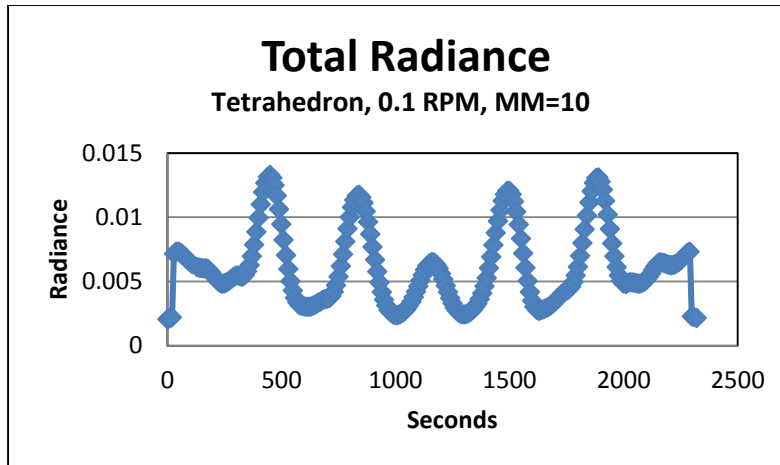
Fig. 10. Total radiance as a function of time for the rotating tetrahedron satellite

A quick look at the radiance curve shows the difference between the peaks ranging from 320 to 390 seconds. A Fast Fourier Transform (FFT) of the radiance curve, as shown in Fig. 11, suggests a rotation rate of 366 seconds.
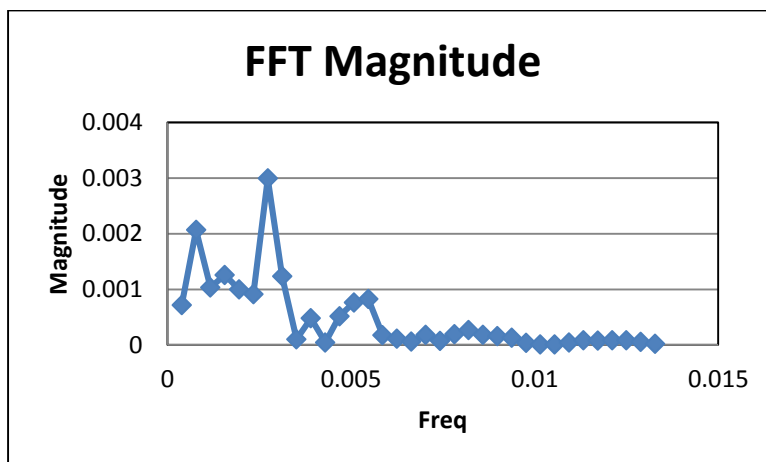

Fig. 11. FFT of the radiance curve for the rotating tetrahedron satellite

Since the tetrahedron is rotating about the nadir pointing end at a rotation rate of 0.1 RPM (or 600 seconds for a full rotation), we should expect the time between peaks, when the facet face is pointed toward the site should be 200 seconds. Clearly, the results are not simple, or could point to an unexpected problem in our rotation calculation. It is no surprise that if the time spacing between spectra is increased, as shown in Fig. 12, that the ability to determine the rotation rate become much more difficult, if not impossible.
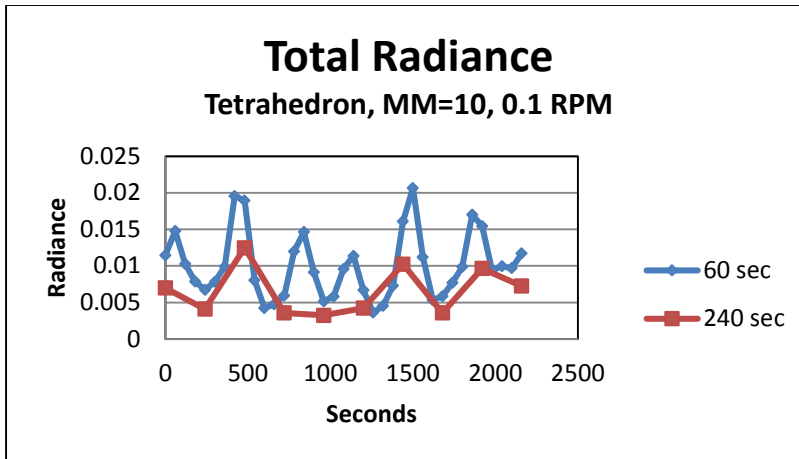
Fig. 12. Tetrahedron at 60 and 240 second spacing

To determine if spectral pattern matching can improve our knowledge of the satellite rotation and attitude, we compute spectral images of the same rotating tetrahedron through a pass over the sensor. For the first test case, we pixilated the image so that some features are visible, as shown in Fig. 13.
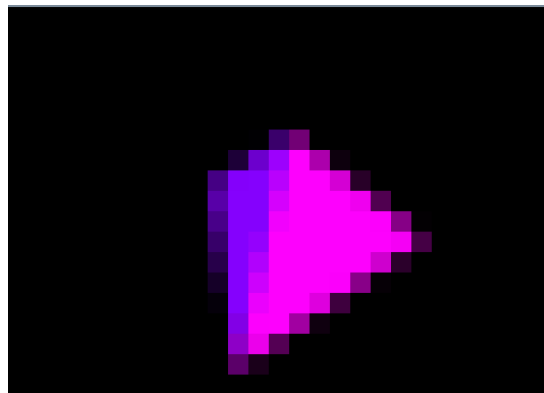

Fig. 13. Pixilated tetrahedron used for initial spectral similarity analysis

To compare the spectra across multiple images, we save a copy of a spectrum from an image and compare to subsequent images using a simple SAM algorithm to evaluate like spectra. The resultant image is gray-scaled to show how close the pixels match the selected spectrum. To further show how close the pixels match the selection, an angular threshold is applied and all pixels that fall within that angular range are highlighted in red. Fig. 14 shows the SAM results with the threshold applied on the initial satellite spectral image.
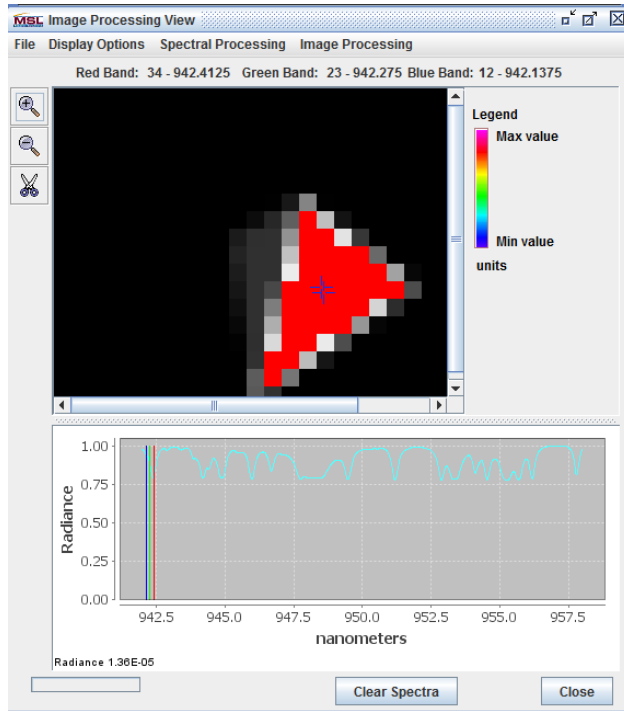
Fig. 14. SAM highlighted results for initial spectral comparison

A spectrum was selected in Fig. 14 and used for comparison to the spectra in Fig. 15. The similar spectra are highlighted. Since this image is rotated from the image in Fig. 14, more of another face is now visible.
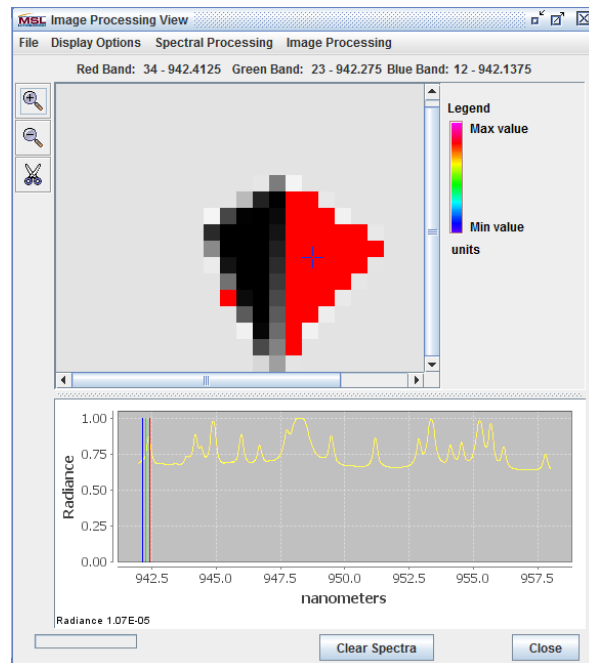

Fig. 15. Rotated image with matching spectra highlighted

Fig. 16 shows the same spectral image as in Fig. 15 with a spectrum on the left hand face, which is dark in the above image selected and highlighted from the SAM analysis.

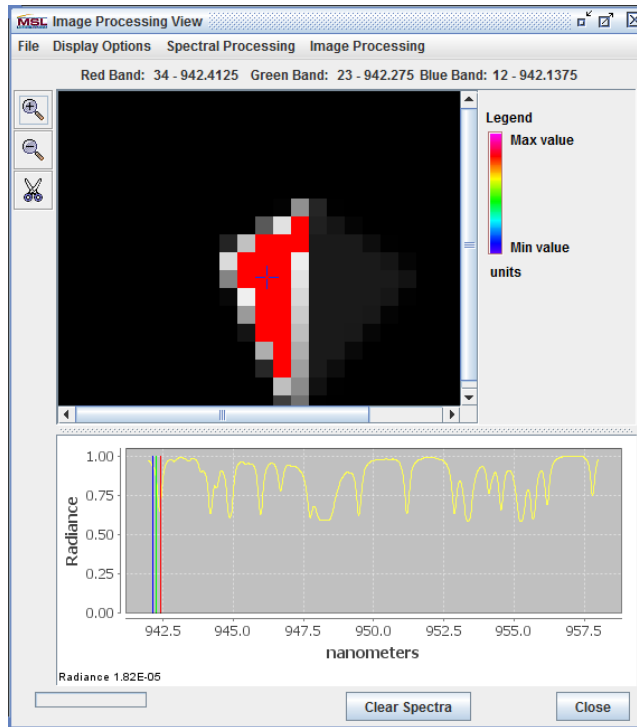**Fig. 16. Matching spectra within image for left side of image**

As the tetrahedron continues to rotate, the face selected in Fig. 16 has rotated into full view, as shown in Fig. 17.
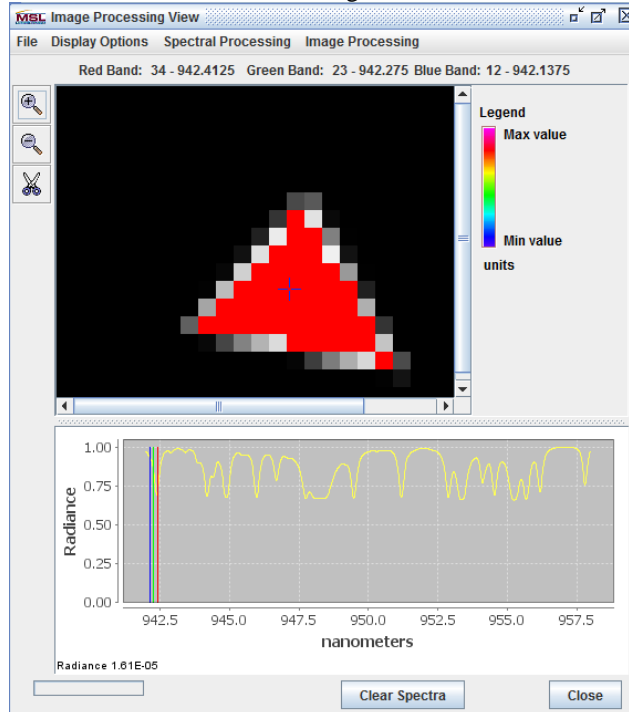

Fig. 17. Matching spectra of face as it rotates into view

SAM results at other time steps within the orbit show the same results as presented here. Using the same SAM threshold value for all images taken along the orbit clearly shows that analyzing the time variability of the spectral signature shows the rotation of the satellite.

For unresolved images, the spectral similarity computations yield some promising results. For this case, we compute the rotating tetrahedron at the same 0.1 RPM as before but with a time step between spectra of 240 seconds. This is the same case as given in Fig. 12 from which it was difficult to determine satellite attitude and rotation. Shown in the sequence of images below are the radiance, pixilated image, spectral similarity image, and an image showing the different satellite materials. From the total radiance alone, we are unable to determine the face type or orientation, but the spectral information enables us to distinguish different materials, even in the unresolved imagery.

The third image in Fig. 18 show similar spectral materials in the red highlighted part of the image. This is confirmed in the fourth image which shows the material map. A spectrum is selected from a pixel in the image and stored for comparison in this and subsequent images. The saved spectrum is a blended spectrum of all the materials in the pixel. Two spectra were saved from the first image to represent the different blends of materials, similar to what was done above, but due to the larger pixels, the spectrum is a composite of multiple materials.
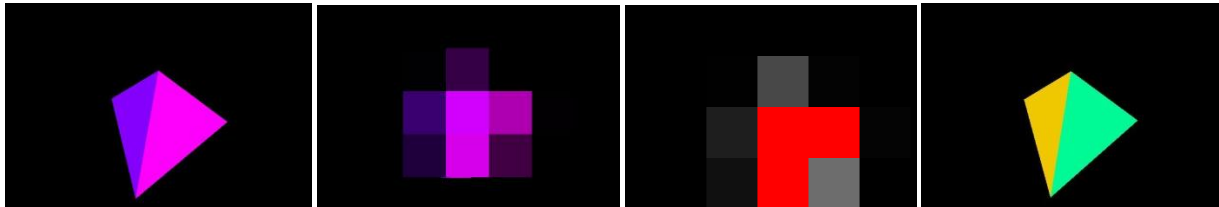

Fig. 18. Unresolved radiance image showing spectral similarity (t=0)

Fig. 19 shows the material face that was colored yellow in the previous sequence rotated to the right of the field-of-view and a new face showing a material that was not visible in Fig. 18 colored in light blue. The similarity image compares the spectrum from the "yellow" material in Fig. 18 to the materials in this image. The pixel blending makes it difficult to find the "yellow" material, but we do see that the pixels on the right hand side of the unresolved image are closer matches, as they should be.

Fig. 19. Radiance, spectral similarity, and material images (t=240 seconds)

At 480 seconds into the simulation (satellite pass), as seen in Fig. 20, the tetrahedron shows a face with materials that were in the original image. The radiance of the image is also very similar to what was seen in Fig. 18. This is a peak in the total radiance curve as seen in Fig. 12. The spectral similarity properly picks out the material in the original image, Fig. 18, as the highlighted area.

Fig. 20. Radiance, spectral similarity, and material images (t=480 seconds)

Fig. 21 shows the match to the "yellow" material spectrum. It corresponds reasonably well to the material image.

Fig. 21. Radiance, spectral similarity, and material images (t=720 seconds)

Fig. 22 shows the spectral match to the light green spectrum from the original image. Through this similarity, we are able to roughly determine which side of the unresolved image corresponds to the selected material.
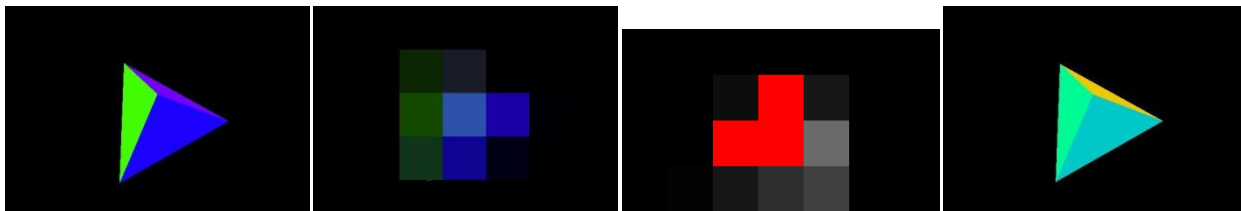

Fig. 22. Radiance, spectral similarity, and material images (t=960 seconds)

Although not conclusive, this series of images and the spectral similarity analysis does yield additional information about the location of materials within the image that would not be seen by a total radiance curve alone.

3. CONCLUSIONS

This study has shown that there is a potential utility in using spectral similarity techniques to help ascertain satellite rotation and attitude. Spectral data adds a dimension that can be exploited by even simple techniques to yield additional insights. Utilizing even a simple technique such as a Spectral Angle Mapper algorithm with threshold highlighting (spectral alarming) on spectral imagery can show an operator more information than is available via broad band imagery. Tracking similar spectra provides additional insight into the behavior of satellites and can assist in their categorization. Other spectral regions where there is a larger variability in the spectral signatures due to the different materials can be expected to yield similar, or even better results than shown here. More sophisticated techniques which extract information on materials within a pixel, such as sub-pixel deconvolution, may also yield improved results. More investigation needs to be performed to understand the bounds of these techniques.

4. REFERENCES

1. Wilkins, Pfeffer, Schumacher, Jah, Towards an Artificial Space Object Taxonomy, draft paper, 2014
2. Coughlin, J. Diagnosing satellite anomalies from time-varying similarity analyses in spectral imagery, Advanced Maui Optical and Space Surveillance Technologies Conference, Maui, HI, September 2008
3. Coughlin, J., Analysis of Atmospheric Impact on the Evaluation of Hyperspectral Imagery, Advanced Maui Optical and Space Surveillance Technologies Conference, Maui, HI, September 2006
4. Coughlin, J., Emission Spectra: A Multi-Purpose Radiative Transfer Environment for Hyperspectral Data Modeling and Exploitation, Proceedings International Symposium on Spectral Sensing Research, Maui, HI, November 1992
5. Coughlin, J., ES: A Fast Line Code, Proceedings Electro-Optical Aerial Targeting Models Users Meeting, Dayton, OH, June 1990

6. Chang, Chien-I, *Hyperspectral Imaging: Techniques for Spectral Detection and Classification*, Klewer Academic/Plenum Publishers, New York, 2003.